Nanoscale

PAPER

View Article Online
View Journal | View Issue

Cite this: *Nanoscale*, 2025, **17**, 5438

A fluorescence nanosensor based on modified sustainable silica for highly sensitive detection of the SARS-CoV-2 IgG antibody†

Firda Apriyani,[a,b] Shaimah Rinda Sari,[c] Himawan Tri Bayu Murti Petrus,[d] Marissa Angelina,[e,f] Robeth V. Manurung,[f,g] Ni Luh Wulan Septiani,[f,h] Brian Yuliarto[a,b,f] and S. N. Aisyiyah Jenie[*c,f]

This study presents an innovative fluorescence nanosensor utilizing modified sustainable silica for the ultra-sensitive detection of SARS-CoV-2 IgG antibodies. The sensor employs fluorescent dye-doped silica nanoparticles (FSNPs) synthesized *via* the sol–gel method and functionalized with rhodamine B as a fluorescent dye. Fourier-transform infrared (FTIR) analysis confirmed the successful immobilization of anti-IgG on the FSNP surface, as evidenced by the characteristic amide I and II peaks at 1641 cm^{-1} and 1530 cm^{-1}, respectively. Detection of SARS-CoV-2 IgG antibodies was achieved through the enhanced fluorescence intensity of FSNP-anti-IgG at 582 nm. Optimal detection conditions were established with a 15-minute incubation period, demonstrating a linear detection range from 10^{-8} to 10^{-2} μg mL^{-1} and a limit of detection (LOD) of 5.3 fg mL^{-1}. This research highlights the potential of modified sustainable silica-based fluorescence nanosensors, particularly those utilizing FSNP-anti IgG, for advancing sensitive, rapid, and cost-effective COVID-19 diagnostics, making them a viable option for pathogen detection in resource-limited settings.

Received 31st October 2024,
Accepted 27th January 2025

DOI: 10.1039/d4nr04546g

rsc.li/nanoscale

Introduction

COVID-19 continues to pose a significant public health concern, requiring advancements in detection, vaccination, and treatment. Since the 2020 outbreak, the virus has undergone multiple mutations, leading to new variants, which have influenced the development of updated vaccines and detection methodologies. The U.S. Food and Drug Administration (FDA) has recommended developing monovalent vaccines targeting the JN.1 lineage for the 2024–2025 season, which aligns with the current circulating strains.[1] These updated vaccines aim to enhance protection against severe diseases caused by the predominant variants. Therefore, researchers are now seeking to develop updated vaccines that will provide immunity against the newest variants. For instance, the updated vaccines for the 2023–2024 period target the Omicron XBB.1.5 subvariant and its related strains. In the same way as the influenza vaccine, these vaccines are updated as the virus evolves.[2] Health officials recommend additional doses for older adults and those with compromised immune systems to maintain high immunity levels.[3] Early and accurate detection of SARS-CoV-2 is critical for controlling the spread of the virus and managing the pandemic.

Conventional diagnostic methods like real-time polymerase chain reaction (RT-PCR) remain the gold standard due to their high sensitivity and specificity.[4] A number of factors, including the long procedure time, certification of laboratories, expensive reagents and equipment, and requirement of well-trained technicians, limit the use of RT-PCR, particularly in rural and isolated areas.[5] The limitations of conventional diagnostic methods have led to the development of alternative tech-

[a]*Master Program of Nanotechnology, Graduate School, Institut Teknologi Bandung, Ganesha 10, Bandung, West Java 40132, Indonesia*
[b]*Advanced Functional Material Research Group, Faculty of Industrial Technology, Institut Teknologi Bandung, Jl. Ganesha No. 10, Bandung, West Java 41032, Indonesia*
[c]*Research Center for Chemistry, National Research and Innovation Agency (BRIN), Kawasan Sains dan Teknologi (KST) B. J. Habibie, Building 452, Serpong, South Tangerang, Banten 15314, Indonesia. E-mail: siti043@brin.go.id*
[d]*Department of Chemical Engineering, Faculty of Engineering, Universitas Gadjah Mada, Jalan Grafika No 2, Yogyakarta, 55281, Indonesia*
[e]*Research Center for Pharmaceutical Ingredients and Traditional Medicine, National Research and Innovation Agency (BRIN), Cibinong Science Center (CSC), Bogor, West Java 16911, Indonesia*
[f]*BRIN and ITB Collaboration Research Center for Biosensor and Biodevices, Jl. Ganesa 10, Bandung, West Java 40132, Indonesia*
[g]*Research Centre for Electronics, National Research and Innovation Agency (BRIN), Kawasan Sains dan Teknologi (KST) Samaun Samadikun, Jl. Cisitu Sangkuriang, Dago, Bandung, West Java 40135, Indonesia*
[h]*Research Centre for Nanotechnology Systems, National Research and Innovation Agency (BRIN), Kawasan Sains dan Teknologi (KST) B. J. Habibie, South Tangerang 15314, Indonesia*

† Electronic supplementary information (ESI) available. See DOI: https://doi.org/10.1039/d4nr04546g

niques, such as lateral flow immunoassays (LFIA) and enzyme-linked immunosorbent assays (ELISA). LFIA, a serological test based on point-of-care (PoC), is a more simplified testing system that can be applied. LFIA qualitatively detects blood samples with a fast response time of about 15 minutes. Although it does not directly confirm the presence of the virus, it provides serological evidence of infection.[6] On the other hand, ELISA is a well-established method that detects antigens and antibodies resulting from the immune response.[7] ELISA assays rely on antigen–antibody interactions in a simple binding to immobilize on a solid surface to form an antigen–antibody complex. Enzymes play a vital role in ELISA by catalyzing reactions that generate detectable signals. In most ELISA assays, enzymes are linked to secondary antibodies, binding to the primary antibodies attached to the antigen of interest. These enzymes facilitate reactions that produce colorimetric, fluorometric, or chemiluminescent signals, enabling the quantification of the antigen–antibody complex.[8] However, conventional ELISA methods are characterized by limitations, particularly in the simultaneous detection of multiple biomarkers. These methods can also be time-consuming[9] and prone to enzyme use problems, such as substrate solution contamination and the need to read the microwell shortly after the enzyme/substrate reaction is completed.[10]

To overcome these limitations, fluorescence-linked immunoassays offer advantages, including increased sensitivity[11] and more excellent stability of reagents.[12] Fluorescence methods also use lower reagent volumes and decrease the assay time.[13] However, challenges are posed by spectroscopically detecting multiple analytes in a single-well assay, such as the cross-reactivity of antibodies and the need for discrete spectral bands that do not overlap too closely.[14] The solution to these challenges is using fluorescent nanoparticles as immunoassay labels. These nanoparticles can overcome some limitations associated with conventional ELISA methods, making them promising tools for detecting biomarkers.[15]

Biosensors are compact devices for detecting important analytes or pathogens in the food industry, environment, and healthcare. An applicable biosensor should fulfill several requirements, including excellent sensitivity and response accuracy, specific targeting, non-toxicity, and cost-effectiveness.[16] Optical biosensors as among the most widely used devices offer an alternative method for virus detection due to their safe, easy-to-use, and cost-effective technology.[17] Optical biosensors operate on the principle of detecting changes in optical properties, such as absorption, fluorescence, or surface plasmon resonance (SPR),[18] induced by the binding of target molecules to recognition elements immobilized on a sensor surface. These recognition elements, including antibodies, aptamers, enzymes, and nucleic acids, selectively capture the target analyte, leading to a measurable signal correlating with its concentration in the sample. Fluorescence-based optical biosensors are highly valued in research and clinical settings due to their unique advantages, including high sensitivity and biocompatibility.[19] These attributes make them particularly effective for detecting various analytes, including viruses and disease biomarkers.[17] Organic fluorescent dyes such as fluorescein isothiocyanate (FITC) and rhodamine B have been widely used in bioimaging and bio-tracing of analytes. However, these dyes deteriorate from photobleaching and are chemically unstable. The incorporation of these dyes into nanoparticles results in a more reliable and sensitive fluorescence signal output. Advances in nanotechnology have provided nanoparticle-based fluorescence sensors with high sensitivity and photostability.[20,21] FSNPs have been widely used for bioimaging and biosensing applications,[22] including cell imaging,[23] detection of bacteria,[24] virus detection,[25] and antibody detection.[26] In addition to high sensitivity and photostability, FSNPs have properties such as high surface area, ability to bind molecules, biodegradability, and low toxicity. Based on these properties, FSNPs can be developed for sensitive detection of biomarkers.[27]

The sol–gel method is the most commonly used method to synthesize FSNPs. It involves acid or base-catalyzed hydrolysis of alkoxide precursors followed by condensation reactions, ultimately forming a gel-like material that includes both solid and liquid phases. The specific process parameters, such as the type of catalyst, significantly influence the structure and properties of the resulting silica network.[28] Chitra *et al.* have reported that the aging process for the synthesis of FSNP is 18 hours at room temperature.[29] This was confirmed by the works of Jenie *et al.*,[30] which showed that the optimum time for aging was 18 hours, resulting in a surface area of 289 m^2 g^{-1}. During aging, continued polycondensation increases the thickness between colloidal particles and decreases porosity. It also enhances the overall stability and surface area of the material. This step is crucial for ensuring the FSNPs achieve the desired structural and functional properties for various applications, including biosensing and imaging.[31] Untoro *et al.* have developed FSNPs, where the silica precursor was derived from modified sustainable silica. FSNPs were synthesized by adding cetyl trimethyl ammonium bromide (CTAB) as a surfactant to form a uniform pore size and rhodamine B as the fluorescent dye.[32] The result showed that rhodamine B is incorporated within the pores of silica nanoparticles, having a uniform pore distribution and surface area of 190.22 m^2 g^{-1}. The FSNP samples also produced a highly fluorescent signal.

Various techniques are commonly used to functionalize silica nanoparticle surfaces, such as layer-by-layer assembly, physisorption, and silane coupling agents (co-hydrolysis). Among them, the hydrosilylation method is widely used to modify silica surfaces. This process involves the thermal, catalytic, or photochemical reaction of alkene chains or double bonds with the silicon surface to form silicon–carbon and hydrogen–carbon bonds. Therefore, the surface functionalized nanoparticle can further be conjugated with biomolecules such as antibodies.[33–35] The current research builds upon previous studies by leveraging fluorescent nanoparticles for the rapid and sensitive detection of biomarkers. These fluorescent nanoparticles have demonstrated exceptional potential in identifying pathogens and antigens with high sensitivity and specificity. Jenie *et al.* have succeeded in detecting *E. coli* bac-

teria using FSNPs as the biosensing platform as low as 8 CFU per mL in the concentration range of 10–10^{-5} CFU per mL.[36] Kurdekar *et al.* used fluorescent silver nanoparticles to develop highly sensitive assays for detecting early HIV infections.[15] This assay was capable of detecting HIV p24 antigen between 10 and 1000 pg mL^{-1} in a linear dose. Kim *et al.* have reported on the antigen-conjugated FSNPs to detect biomarkers with an immobilized-antigen immunofluorescence glass slide system.[37] The results showed the increasing fluorescence intensity due to the formation of a complex between the antigen and bioconjugate in the 0.1 to 0.25 mg mL^{-1} range. Another study by Kasetsirikul *et al.* has described the detection of SARS-CoV-2 antibodies within 30 minutes using the ELISA method.[8] This rapid detection capability is crucial for the timely diagnosis and management of COVID-19. Apriyani *et al.* have successfully modified FSNPs based on natural silica to detect IgY antibodies using the ELISA method with a detection time of 60 minutes.[26] The fluorescence intensity of the FSNP-anti IgY nanoprobe decreased upon detecting the IgY antibody, demonstrating that modified FSNPs with anti-IgY can effectively detect antibodies based on fluorescence. These studies collectively highlight the potential of fluorescence nanoparticles as powerful tools for biomarker detection, offering high sensitivity, specificity, and versatility across various applications.

This research focuses on the latest updates in COVID-19 management and applying a fluorescence nanosensor for ultrasensitive SARS-CoV-2 IgG antibody detection using modified sustainable silica. In this study, an innovative approach of using silica from geothermal precipitate as a natural and environmentally friendly precursor was used for the synthesis of nanoparticles to minimize the ecological impact. A surface-modified fluorescent silica nanoparticle (FSNP) is applied in this study as a biosensing platform for detecting SARS-CoV-2 IgG antibodies. The fluorescent nanostructures were synthesized from geothermal silica *via* the sol–gel method and subsequently modified with rhodamine B as a fluorophore.[36] The surface of the FSNP was characterized by Fourier transform infrared (FTIR) spectroscopy, the Brunauer–Emmett–Teller (BET) method, scanning electron microscopy (SEM), and X-ray diffraction (XRD). A fluorescence immunoassay is used to detect IgG antibodies, and the LOD value is calculated using the linearity of the FSNP-anti IgG fluorescence intensity while detecting antibodies.

Experimental

Materials

The geothermal precipitate was obtained from Geodipa Power Plant, Central Java, Indonesia as the silica precursor. Sodium hydroxide (NaOH), hydrochloric acid (HCl 37%), undecylenic acid, *n*-hydroxy succinimide (NHS), and cetyltrimethylammonium bromide (CTAB) were purchased from Merck Chemicals (Darmstadt, Germany). Phosphate-buffered saline (PBS), rhodamine B, Tween-20, and 1-(3-dimethyl aminopropyl)-3-ethylcarbodimide (EDC) were purchased from Sigma Aldrich (St Louis, MO, USA). SARS-CoV-2 IgG nucleocapsid antibody [6H3] (mouse monoclonal antibody) and goat anti-mouse IgG (Fc fragment) antibody [RMG06] were purchased from GeneTex (Irvin, CA, USA). All chemicals were used without further purification and reagents were prepared with deionized water.

Preparation of FSNPs

The method used to synthesize FSNPs is based on our previous work.[36,38] A total of 10 g washed silica powder was mixed and heated at 90 °C with 400 mL of 1.5 N NaOH to form sodium silicate, and then stirred for 1 hour at room temperature. Subsequently, 2.5 mg g^{-1} of rhodamine-B dye was mixed with the sodium silicate solution and titrated with 2 N HCl to form the gel under acidic conditions (pH 5). The gel was immersed in 2 wt% of CTAB in aquadest and aged for 18 hours at room temperature. After the aging process, the gel was washed with aquadest until neutral pH. The sample was then oven-dried at 100 °C for 24 hours to obtain FSNPs.

Surface modification of FSNP

The surface modification of FSNPs aims to activate the chemical groups on the surface to immobilize the SARS-CoV-2 anti-IgG antibody as bio-receptors (Fig. 1). The first modification step was the hydrosilylation reaction. 1 g of FSNP sample was immersed in 7 mL undecylenic acid in a round bottom flask and stirred at 120 °C for 3 hours. The decanted mixture was washed with ethanol 3 times and dried at room temperature overnight. The product of this process was denoted as the FSNP-COOH sample. Subsequently, 1 mg of FSNP-COOH was dissolved in 1 mL of PBS solution and sonicated for 10 minutes. Then, 10 μL of 10 mg mL^{-1} EDC and 100 μL of 5 mg mL^{-1} NHS in PBS were added. The sample was mixed for 30 minutes and centrifuged at 10 000 rpm for 20 minutes, obtaining the FSNP-NHS sample. In the final surface modification step, 1 mg of FSNP-NHS in 250 μL PBS was added with 25 μL of 10 μg mL^{-1} anti-IgG. The sample was mixed for 1 hour, then centrifuged at 10 000 rpm for 10 min

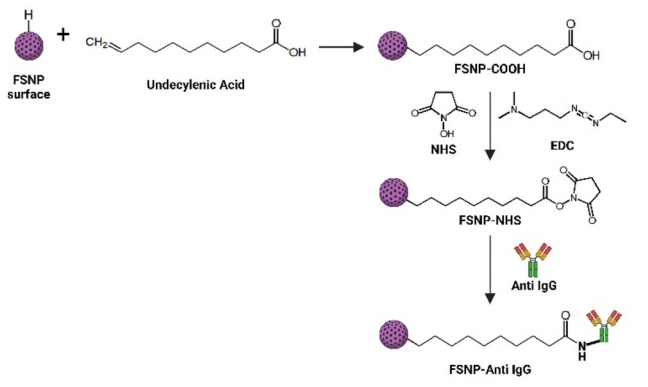

Fig. 1 Modification process on the functionalization of FSNP-anti IgG.

for drying at room temperature. The finished product was labelled as FSNP-anti IgG.

Characterization of FSNPs and FSNP-anti-IgG

XRD patterns were recorded using a secondary graphite monochromator (Rigaku Miniflex, Rigaku, Japan) with (Cu Kα) radiation at 40 kV and 30 mA. The morphology of the nanoparticles was obtained using field emission scanning electron microscopy (FESEM) measurements (Hitachi SU3500, Japan). The FESEM-EDS images were obtained with a JIB-4610F equipped with a Schottky electron gun and a new FIB column capable of sizeable current processing with a maximum ion current of 90 nA installed into one chamber. The software used to generate spectra was IR solution (Shimadzu, Japan). Nitrogen adsorption–desorption isotherms were recorded on a NOVA 2200e surface area and pore size analyzer (Quantachrome, USA). Before each measurement, all samples were degassed at 150 °C for six hours to remove the physisorbed moisture. FTIR characterization was carried out by using an FTIR Prestige-21 (Shimadzu, Japan) in transmittance mode at 16 cm^{-1} resolutions over the range of 400–4500 cm^{-1} with an accumulating average of 10 scans. The fluorescence intensity was measured using a Varioskan Flash Spectral Scanning Multimode Reader (Thermo Scientific, Finland) at an excitation wavelength of 545 nm and an emission range of 550–600 nm.

Immunoassay protocol for SARS-CoV-2 IgG antibody detection

The SARS-CoV-2 IgG antibody was detected by the changes in the fluorescence intensity at a 582 nm emission peak using 100 μL at various concentrations, which were added to the well plate and incubated at 4 °C overnight. The concentration of the antibody was varied from 10^{-8} to 10^{-2} μg mL^{-1}. Following this, the plate was washed three times with 100 μL of washing buffer, which was prepared by diluting 0.5 mL Tween-20 into 1 L PBS. After the target had been coated on the well, 200 μl of blocking solution made from 1% bovine serum albumin (BSA) in PBS was used to block the non-specific binding of antibodies and incubated for 1 hour. The unattached targets were removed throughout the washing process. After washing, 100 μL of 0.5 μg mL^{-1} FSNP-anti-IgG was added to the plate to detect the target, incubated for 15 min, and washed 3 times to ensure that only IgG-COVID-19 bound with FSNP-anti IgG. The final step was adding 100 μL PBS to the well, and the maximum fluorescence intensity was examined at 582 nm with excitation at 545 nm (Fig. 2).

LOD was obtained by varying the concentration of the SARS-CoV-2 IgG antibody. First, SARS-CoV-2 IgG antibodies were detected by calculating the normalized fluorescence intensity by subtracting the maximum (I_{max}) intensity and the minimum (I_{min}) intensity. The percentage of normalized intensity was calculated using the following equation:

$$\%\text{Normalized} = ((I_{max} - I_{min})/I_{min}) \times 100\% \quad (1)$$

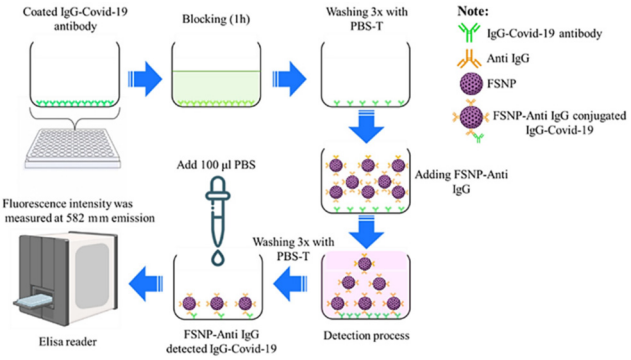

Fig. 2 Detection scheme of SARS-CoV-2 IgG antibody through fluorescence.

the I_{max} and I_{min} represent the maximum fluorescence intensity of FSNP-anti IgG before and after detecting the SARS-CoV-2 IgG antibody for 15 min incubation. The measurements were conducted in triplicate. The standard deviation of three measurement data to plot the error bars was calculated using the equation as follows:

$$SD = \sqrt{\left(\sum (x_i - \bar{x})^2/(n1)\right)} \quad (2)$$

where $\sum$ represents the sum of all data points, x_i represents each data point, $\bar{x}$ represents the sample mean, and n represents the number of data points in the sample. Finally, LOD was calculated using the equation as follows:

$$y\text{LoD} = y\text{b} + 3\text{STDb} \quad (3)$$

where yb is the mean fluorescence intensity loss measured for the blank control, and STBb is the associated standard deviation.[39]

Results and discussion

Characterization of FSNPs

This study synthesized FSNPs using natural silica precursors and rhodamine B as a fluorescent dye using a sol–gel method in which precipitated silica was treated with NaOH to yield sodium silicate. The formed sodium silicate then reacted with HCl as an acid catalyst to form a gel.[27] In the case of FSNPs, the covalent attachment of rhodamine B ensures that it remains within the silica matrix and does not leak out.[40] The crystallinity of the FSNP sample was characterized by XRD. As shown in Fig. 3, the diffraction pattern of FSNP formed a broad peak at 2θ = 22.56, indicating that the fluorescent nanoparticles were in an amorphous phase.[37]

SEM and SEM-EDS were performed to investigate the morphology and components contained in the FSNP samples. Fig. 4 shows the SEM images of FSNPs which are further described in Table S1.† The FSNP sample was primarily composed of silica (Si) at 69.8 wt%, oxygen (O) at 15.4 wt%, and carbon (C) at 13.3 wt%. The average particle size of the FSNPs, as determined by SEM analysis, was 294 nm (Fig. S1†). Additionally, CTAB was

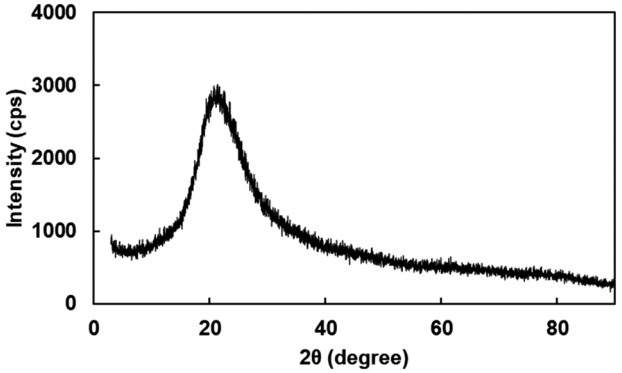

Fig. 3 X-ray diffraction pattern of the FSNP sample.

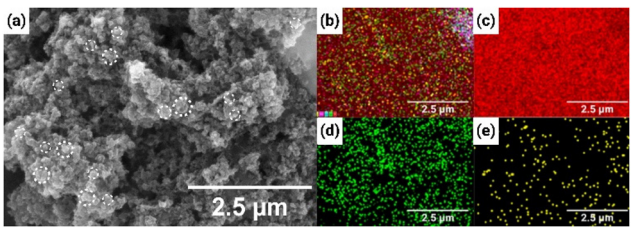

Fig. 4 (a) SEM images of the FSNP sample and energy-dispersive X-ray spectroscopy of FSNP showing total layered (b) and mapping analysis of the layer of Si (c), layer of O (d), and layer of C (e). The incident electron beam was at 90 nA.

used as a template surfactant for the synthesis of FSNP samples in order to produce uniformly sized nanoparticles. The measurement of the FSNP calculated by the BET method resulted in a surface area of 208.95 m^2 g^{-1}. A Barrett–Joyner–Halenda (BJH) analysis of the FSNP samples revealed a cumulative pore volume of 0.578 cm^3 g^{-1} and an average pore size of 19.051 Å. Given these intrinsic properties of the nanoparticles, the FSNP was sufficient for chemical modification and further biomolecule immobilization on its surface.

Surface modification of FSNPs and their functionalization on anti-IgG

Functional groups were identified in the samples before and after surface immobilization with anti-IgG antibody as the bioreceptor *via* FTIR analysis. The FTIR spectra of FSNPs at every stage of modification and functionalization are displayed in Fig. 5. The absorption peaks at 1089 cm^{-1} and 810 cm^{-1} correspond to the symmetric and asymmetric Si–O–Si stretching bonds, respectively, while the absorption peak at 958 cm^{-1} indicates the presence of Si–O bonds.[29] The spectrum of the FSNP-COOH showed peaks at a wavenumber of 1710 cm^{-1}, indicating the presence of the stretching C═O bond of the carboxylic acid. This reaction also produced peaks at wavenumbers 2922 cm^{-1} and 2848 cm^{-1}, showing the presence of C–H bonds derived from undecylenic acid.[41,42]

The spectrum of the FSNP-NHS sample is shown in Fig. 5(c). The disappearance of the peak at 1710 cm^{-1} indicates

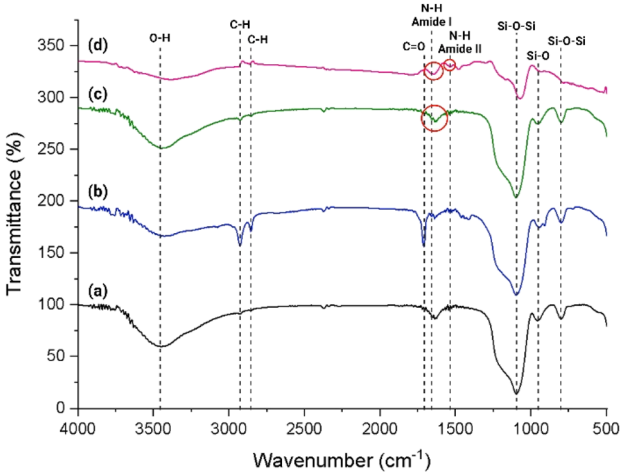

Fig. 5 FTIR spectra of (a) FSNP, (b) FSNP-COOH, (c) FSNP-NHS, and (d) FSNP-anti IgG in transmittance mode.

the reaction of carboxylic acids with EDC and NHS was successful.[43] In this step, a –COO surface is obtained by reacting a surface carboxyl group with EDC and NHS, which act as coupling agents. This process, known as surface activation, forms a succinimidyl ester from the NHS. In particular, one may notice a small broadband at 1639 cm^{-1} in spectra C. These bands are intensely evocative of amide bonds. Amide bonds in FSNP-EDC-NHS reactions are due to the incomplete activation reaction of succinimidyl ester termination to acid groups characterized by a remaining acid C═O vibration at 1715 cm^{-1}. Subsequently, this ester reacts with the amine group on anti-IgG to form FSNP-anti IgG.[44,45] The FTIR spectrum of FSNP functionalized with the anti-IgG antibody is displayed in Fig. 5(d). Peaks at wavenumbers 1641 cm^{-1} and 1530 cm^{-1} correspond to amide I and amide II bonds, respectively, showing the successful immobilization of the anti-IgG antibody to the FSNP surface. Amide II bonds are primarily created by combining N–H bending and C–N stretching vibrations. In contrast, amide I bonds are formed by the C═O stretching vibrations of peptide bonds in the protein backbone.[35]

Detection of the SARS-CoV-2 IgG antibody

A fluorescence immunoassay (FIA) scheme can be seen in Fig. 2, which depicts a biochemical procedure for detecting antibodies by fluorescence. It is an alternative to the ELISA method, substituting an enzyme with a fluorescent label. In this process, a secondary antibody or anti-IgG specific to IgG is conjugated with a fluorescent label FSNP to be FSNP-anti IgG to bind the target or IgG-COVID-19, in this case. The bound FSNP-anti IgG is excited with light at a specific excitation of 545 nm, and the emitted fluorescence is measured at an emission of 582 nm (Fig. S2†). The fluorescence intensity is directly proportional to the amount of IgG antibody in the sample. Using fluorescent labels allows for significant signal amplification and makes detecting small quantities of the target antibody possible.[46]

The sensor fluorescence intensity was measured before and after the detection process. A 5-fold increase in fluorescence intensity was observed after the detection of the SARS-CoV-2 IgG antibody (Fig. S3†). This increase in fluorescence intensity indicates the successful binding and detection of the IgG-COVID-19 antibody and demonstrates the sensor's efficacy in identifying the presence of the target antibody. The increase in fluorescence intensity observed in modified sustainable silica nanosensors after detection may be attributed to several factors. Initially, when SiNPs are functionalized with recognition elements (in this case, IgG antibodies against SARS-CoV-2), they come in close proximity to the analyte. A transfer of energy occurs between the excited state of the recognition element and the SiNPs, resulting in enhanced fluorescence. The binding of IgG antibodies and fluorophores in FSNP facilitates Förster resonance energy transfer (FRET) between fluorophores. The proximity of the IgG can optimize the distances between donor and acceptor fluorophores, improving the energy transfer efficiency.[47,48] The energy transfer from donor to acceptor fluorophores effectively reduces the donor fluorophore's non-radiative decay pathways and increases its quantum yield. The increase in quantum yield will enhance the fluorescence intensity of the FSNPs.[49] As a consequence of the modification of silica surfaces, the local environment surrounding fluorophores is also altered. Not only quantum yields but also fluorescence lifetimes can be altered by this effect, ultimately affecting the overall fluorescence intensity. In the presence of a silica matrix, nanoscale confinement may enhance fluorescence by restricting molecular motion and reducing nonradiative decay pathways.

The analytical performance of FSNP-anti IgG in detecting antibodies was further investigated. The optimum detection response time was determined by varying the incubation times at a constant concentration of 0.01 μg mL^{-1} SARS-CoV-2 IgG antibody. As shown in Fig. 6, the fluorescence intensity value is largely stable between 5 and 10 minutes and increases at 15 minutes. Longer incubation times showed that the intensity decreased. Hence, the optimum response time for FSNP-anti IgG to identify the targets is 15 minutes. To determine the sensitivity and LOD value of FSNP-anti IgG as a biosensing platform, the concentration was varied, ranging from 10^{-8} to 10^{-2} μg mL^{-1}. Using the optimum 15-minute incubation time, the fluorescence intensity at 582 nm was observed for each concentration. The analytical results demonstrated that FSNP-anti IgG effectively binds to the SARS-CoV-2 IgG antibodies, allowing for accurate fluorescence-based detection. Fig. 7(a) shows that the fluorescence intensity of FSNP-anti IgG decreases linearly with the reduction in antibody concentrations. Additionally, Fig. 7(b) illustrates the correlation between the normalized intensity of FSNP-anti IgG at 582 nm and SARS-CoV-2 IgG antibody concentrations, further confirming the sensor's sensitivity and providing a clear relationship between antibody concentration and fluorescence response. The higher intensity values confirm successful detection by the FSNP-anti IgG surface after targeting, as compared to the control group.[50] The highest intensity value observed was 493 a.u. at a concentration of 10^{-2} μg mL^{-1}, whereas the lowest intensity value was 151 a.u. at 10^{-8} μg mL^{-1} SARS-CoV-2 IgG antibody. These results indicate that the FSNP-anti IgG can be effectively used as a detection system, capable of detecting target concentrations as low as 10^{-8} μg mL^{-1}.

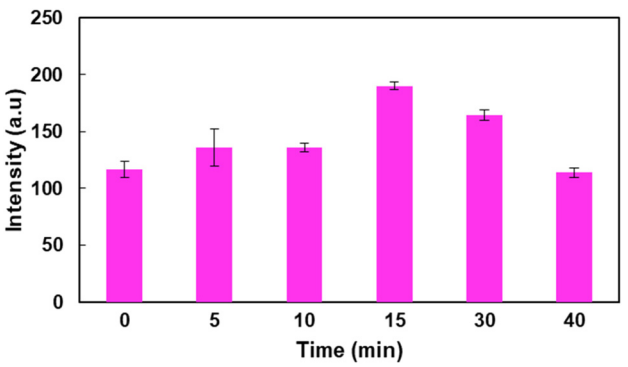

Fig. 6 The fluorescence intensity of 0.5 μg mL^{-1} FSNP-anti IgG in the presence of 0.01 μg mL^{-1} SARS-CoV-2 IgG antibody after the corresponding incubation time with 545 nm excitation and 582 nm emission.

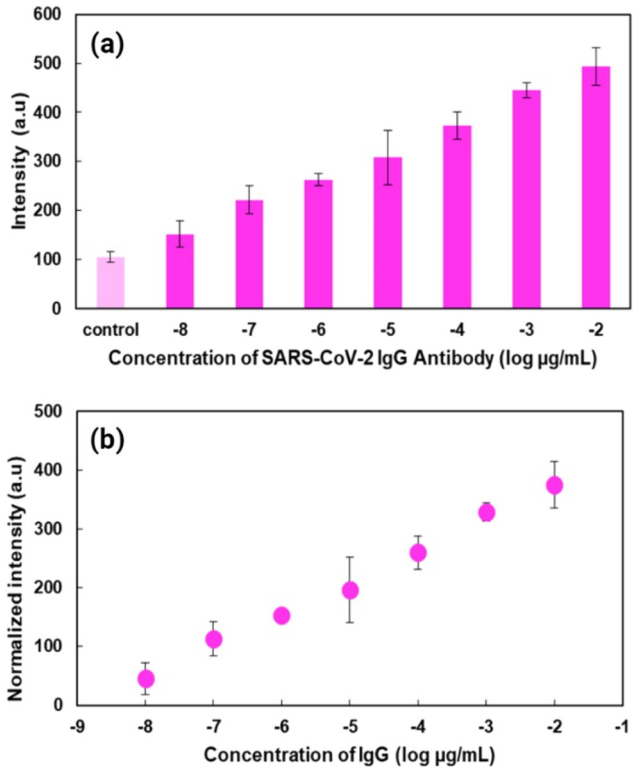

Fig. 7 Fluorescence detection results for FSNP-anti IgG by varying SARS-CoV-2 IgG antibody concentrations. (a) The fluorescence intensity of FSNP-anti IgG (0.5 μg mL^{-1}) in the presence of SARS-CoV-2 IgG antibody (10^{-8} to 10^{-2} μg mL^{-1}) after 15 min of incubation time with 545 nm excitation and 582 nm emission and (b) the correlation between normalized intensity of FSNP-anti IgG at 582 nm and SARS-CoV-2 IgG antibody concentrations after 15 minutes of incubation time. All measurements were made in triplicate.

Table 1 Comparison of different methods for the detection of antibodies

Methods	Target	Material	Incubation time (min)	LOD	Ref.
ELISA	Human IgG antibody	Mesoporous SiNP[a]	30	0.5 ng mL^{-1}	51
ELISA	Human IgG antibody	AuNP[b]	15	0.3 ng mL^{-1}	43
ELISA	Mouse-IgG antibody	Cu-MOF[c]	40	0.34 ng mL^{-1}	52
SPR	SARS-CoV 2	Gold nanospike	30	0.08 ng mL^{-1}	53
LFIA	Anti-SARS-CoV-2 IgG	Selenium nanoparticles	10	5 ng mL^{-1}	54
LFIA	Anti-SARS-CoV-2 IgG dan IgM	Superparamagnetic nanoparticles	10	5 and 15 ng mL^{-1}	55
LFIA	SARS-CoV-2	AuNP[b]	20	0.1 ng mL^{-1}	56
Fluorescence immunoassay	SARS-CoV-2 IgG antibody	FSNP	15	5.3 fg mL^{-1}	**This work**

[a] Mesoporous SiNP: mesoporous silica nanoparticles. [b] AuNP: gold nanoparticles. [c] Cu-MOF: copper-based metal–organic framework.

To calculate LOD and determine the sensitivity of biosensor, a linear correlation was established in the range of 10^{-2} to 10^{-8} μg mL^{-1}. The relationship is described by eqn (1) where normalized intensity = 56.66 log(SARS-CoV-2 IgG antibody) + 501.4 with R^2 = 0.9944, as shown in Fig. 7(b). Using eqn (3) where *y*b is the mean fluorescence intensity measured for the blank control and STDb is the associated standard deviation, LOD was determined to be 5.3 fg mL^{-1}. Accordingly, the FSNP-anti IgG shows an excellent performance in detecting SARS-CoV-2 IgG antibodies. The comparison to other previous works utilizing optical biosensors for the detection of various antibodies is shown in Table 1.

Although the preparation of the test sample and the addition of FSNP-anti IgG require careful handling and precise timing, one significant advantage of our FSNP-anti IgG method over ELISA is its cost-effectiveness. ELISA reagents and kits are notably expensive depending on the complexity and specificity required.[57] In contrast, our method employs inexpensive materials such as silica precursors and rhodamine B, significantly reducing the overall cost. This makes our approach more accessible and straightforward, especially in resource-limited settings where the high cost of ELISA reagents can be prohibitive. Other biosensors offer high sensitivity and rapid detection,[58] yet they often require sophisticated instrumentation, skilled personnel, and tedious washing steps which often compromise the specificity. Optical chips, although providing high sensitivity,[59–61] tend to be more expensive and complex to fabricate. The fluorescence nanosensor utilizing FSNP-anti IgG strikes a balance of sensitivity, speed, and cost-effectiveness, rendering it a viable option for pathogen detection, particularly in resource-limited settings.

Specificity of FSNP-anti IgG

Fig. 8 shows the specificity performance of FSNP-anti IgG biosensors by comparing their responses to various targets including *E. coli*, chicken IgY, SAA, and human-IgG antibodies. The data show that the biosensor's response intensity to the SARS-CoV-2 IgG antibody is significantly higher, reaching 429 a.u. In contrast, the responses to *E. coli*, Chicken IgY, SAA, and human-IgG antibodies are nearly identical to the control (*i.e.* FSNP-anti IgG) and considerably lower than the response to the SARS-CoV-2 IgG antibody. This significant difference in response intensity demonstrates that FSNP-anti IgG biosensors exhibit excellent selectivity for the target SARS-CoV-2 IgG antibody, distinguishing it from other non-target substances tested.

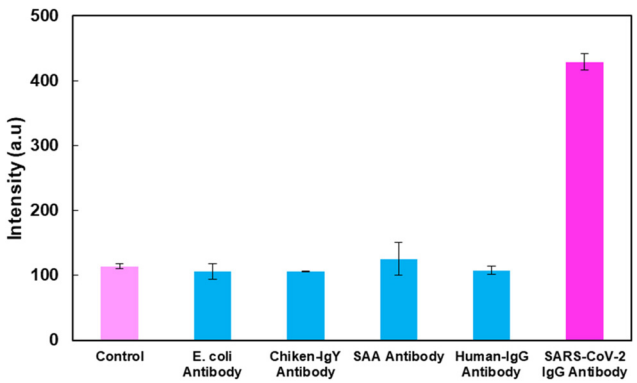

Fig. 8 Specificity of the FSNP-anti IgG (0.5 μg mL^{-1}) towards SARS-CoV-2 IgG antibody compared to *E. coli*, chicken IgY, SAA, and human IgG antibody. All target concentrations were made to 0.01 μg mL^{-1} with 15 minutes of incubation time and 545 nm excitation and 582 nm emission. All measurements were made in triplicate.

Conclusions

This research successfully developed a fluorescence nanosensor using modified sustainable silica for the ultrasensitive detection of SARS-CoV-2 IgG antibodies. FSNPs were successfully synthesized using the sol–gel method with sustainable silica as a precursor and rhodamine B dye and obtained a surface area of 208.956 cm^2 g^{-1} through an amorphous phase. The surface functionalization of FSNP-anti IgG has been successfully carried out using a hydrosilylation reaction and modification using the EDC and NHS and confirmed by FTIR analysis that shows amide I and II groups at wavenumbers 1641 cm^{-1} and 1530 cm^{-1}.

The fluorescence immunoassay demonstrated that the FSNP-anti IgG platform could detect SARS-CoV-2 IgG antibodies at concentrations as low as 10^{-8} μg mL^{-1} with an LOD value of 5.3 fg mL^{-1} in 15 minutes response time. This study underscores the potential of FSNP-based fluorescence nanosensors in enhancing COVID-19 diagnostic strategies, providing a rapid, sensitive, and specific detection method. Future research could focus on optimizing the sensor for point-of-care applications and exploring its applicability in detecting real samples and other biomarkers, further advancing the field of biosensing technology.

Author contributions

Firda Apriyani: methodology, investigation, data curation, formal analysis, and writing – original draft. Shaimah Rinda Sari: writing – review & editing, visualization, validation, and investigation. Himawan Tri Bayu Murti Petrus: resources, formal analysis, investigation, and validation. Marissa Angelina: resources, formal analysis, investigation, and validation. Robeth V. Manurung: resources, formal analysis, investigation, and validation. Ni Luh Wulan Septiani: resources, formal analysis, investigation, and validation. Brian Yuliarto: validation, funding acquisition, supervision, conceptualization, and project administration. S. N. Aisyiyah Jenie: writing – review & editing, validation, funding acquisition, supervision, conceptualization, methodology, and project administration.

Data availability

The data supporting this article have been included as part of the ESI.†

Conflicts of interest

There are no conflicts to declare.

Acknowledgements

The authors would like to acknowledge financial support from the JFS SEA-EU/NAPARBA project Grant No. SEA-EUROPE JFS19ST-117, the BRIN Riset dan Inovasi untuk Indonesia Maju (RIIM) and the Indonesian Endowment Fund for Education (LPDP) Grant No. B-844/II.7.5/FR.06/5/2023 dan no. B-948/III.10/FR.06/5/2023. The authors acknowledge the facilities, scientific, and technical support from the Advance Characterization Laboratories of the National Research and Innovation Agency (BRIN) through E-Layanan Sains. S. N. A. J. is the main contributor to this manuscript.

References

1 U.S. Food and Drug Administration, Vaccines, Blood & Biologics, Updated COVID-19 Vaccines for Use in the United States Beginning Fall 2024, 2024, **https://www.fda.gov/vaccines-blood-biologics/updated-covid-19-vaccines-use-united-states-beginning-fall-2024/** (accessed February 2024).
2 K. Katella, Yale Medicine, Family Health, 10 Things to Know About the Updated COVID-19 Vaccines, 2024, **https://www.yalemedicine.org/news/updated-covid-vaccine-10-things-to-know/** (accessed July 2024).
3 L. Panagiotakopoulos, M. Godfrey, D. L. Moulia, R. Link-Gelles, C. A. Taylor, K. Chatham-Stephens, O. Brooks, M. F. Daley, K. E. Fleming-Dutra and M. Wallace, Updated Recommendations for COVID-19 Vaccination, Centers for Disease Control and Prevention, 2024, 73, 16, 377–381. **https://www.cdc.gov/mmwr/volumes/73/wr/mm7316a4.htm/** (accessed July 2024).
4 J. Zhao, Q. Yuan, H. Wang, W. Liu, X. Liao, Y. Su, X. Wang, J. Yuan, T. Li, J. Li, S. Qian, C. Hong, F. Wang, Y. Liu, Z. Wang, Q. He, Z. Li, B. He, T. Zhang, Y. Fu, S. Ge, L. Liu, J. Zhang, N. Xia and Z. Zhang, *Clin. Infect. Dis.*, 2020, **71**, 2027–2034.
5 S. Marino, M. Ruggieri and R. Falsaperla, *Med. Hypotheses*, 2020, **144**, 110041.
6 Z. Li, Y. Yi, X. Luo, N. Xiong, Y. Liu, S. Li, R. Sun, Y. Wang, B. Hu, W. Chen, Y. Zhang, J. Wang, B. Huang, Y. Lin, J. Yang, W. Cai, X. Wang, J. Cheng, Z. Chen, K. Sun, W. Pan, Z. Zhan, L. Chen and F. Ye, *J. Med. Virol.*, 2020, **92**, 1518–1524.
7 R. Kumar, S. Nagpal, S. Kaushik and S. Mendiratta, *VirusDisease*, 2020, **31**, 97–105.
8 S. Kasetsirikul, M. Umer, N. Soda, S. K. Rajan, M. J. A. Shiddiky and N. T. Nguyen, *Analyst*, 2020, **145**, 3201–3207.
9 S. Pang, J. Smith, D. Onley, J. Reeve, M. Walker and C. Foy, *J. Immunol. Methods*, 2005, **302**, 1–12.
10 G. P. Rai and K. S. Venkateswaran, *Def. Sci. J.*, 1992, **42**, 71–84.
11 L. M. Lei, Y. S. Wu, N. Q. Gan and L. R. Song, *Clin. Chim. Acta*, 2004, **348**, 177–180.
12 J. Y. Hou, T. C. Liu, G. F. Lin, Z. X. Li, L. P. Zou, M. Li and Y. S. Wu, *Anal. Chim. Acta*, 2012, **734**, 93–98.
13 T. B. Martins, N. H. Augustine and H. R. Hill, *J. Immunol. Methods*, 2006, **316**, 97–106.
14 K. Murray, Y. C. Cao, S. Ali and Q. Hanley, *Analyst*, 2010, **135**, 2132–2138.
15 A. D. Kurdekar, L. A. A. Chunduri, S. M. Chelli, M. K. Haleyurgirisetty, E. P. Bulagonda, J. Zheng, I. K. Hewlett and V. Kamisetti, *RSC Adv.*, 2017, **7**, 19863–19877.
16 Z. Rezaei and M. Mahmoudifard, *J. Mater. Chem. B*, 2019, **7**, 4602–4619.
17 A. Arranz and J. Ripoll, *Front. Pharmacol.*, 2015, **6**, 189.
18 J. Homola, *Chem. Rev.*, 2008, **108**, 462–493.

19 R. Hu, T. Liao, Y. Ren, W. Liu, R. Ma, X. Wang, Q. Lin, G. Wang and Y. Liang, *Nano Res.*, 2022, **15**, 7313–7319.
20 P. D. K. P. Ananda, A. Tillekaratne, C. Hettiarachchi and N. Lalichchandran, *Appl. Surf. Sci. Adv.*, 2021, **6**, 100159.
21 H. Luo, L. Tian, Y. Zhang, Y. Wu, B. Li and J. Liu, *Nano Res.*, 2024, **17**, 6443–6474.
22 B. Song and Y. He, *Nano Today*, 2019, **26**, 149–163.
23 C. Yang, T. Li, Q. Yang, Y. Guo and T. Tao, *Spectrochim. Acta, Part A*, 2022, **273**, 121048.
24 D. A. Widyasari, D. Julyansyah, A. Kristiani, B. A. Widyaningrum, H. T. B. M. Petrus, R. V. Manurung and S. N. A. Jenie, *AIP Conf. Proc.*, 2021, **2021**, 030009.
25 Y. Xue, C. Liu, G. Andrews, J. Wang and Y. Ge, *Nano Convergence*, 2022, **9**, 15.
26 F. Apriyani, D. Julyansyah, M. Angelina, A. Randy, R. V. Manurung, B. Yuliarto and S. N. A. Jenie, *J. Metastable Nanocryst. Mater.*, 2023, **35**, 19–24.
27 Y. M. Untoro, D. A. Widyasari, E. Supriadi and S. N. A. Jenie, *J. Pure Appl. Chem. Res.*, 2020, **9**, 171–176.
28 V. Gubala, G. Giovannini, F. Kunc, M. P. Monopoli and C. J. Moore, *Cancer Nano*, 2020, **11**, 1.
29 K. Chitra and G. Annadurai, *J. Nanotechnol.*, 2013, **2013**, 1–7.
30 S. N. A. Jenie, A. Ghaisani, Y. P. Ningrum, A. Kristiani, F. Aulia and H. T. M. B. Petrus, *AIP Conf. Proc.*, 2018, **2026**, 020008.
31 N. Baig, I. Kammakakam and W. Falath, *Mater. Adv.*, 2021, **2**, 1821–1871.
32 E. Yasun, C. Li, I. Barut, D. Janvier, L. Qiu, C. Cui and W. Tan, *Nanoscale*, 2015, **7**, 10240–10248.
33 V. Loryuenyong, T. Muanghom, T. Apinyanukul and P. Rutthongjan, *Adv. Appl. Ceram.*, 2011, **110**, 335–339.
34 S. N. A. Jenie, S. E. Plush and N. H. Voelcker, *Pharm. Res.*, 2016, **33**, 2314–2336.
35 K. Khaldi, S. Sam, A. Lounas, C. Yaddaden and N. E. Gabouze, *Appl. Surf. Sci.*, 2017, **421**, 148–154.
36 S. N. A. Jenie, Y. Kusumastuti, F. S. H. Krismastuti, Y. M. Untoro, R. T. Dewi, L. Z. Udin and N. Artanti, *Sensors*, 2021, **21**, 881.
37 N. Kim, S. M. Oh, C. T. Kim, C. J. Kim and Y. J. Cho, *Procedia Food Sci.*, 2011, **1**, 7–11.
38 N. O. Sifana, N. L. W. Septiani, A. W. Septama, R. V. Manurung, B. Yuliarto and S. N. A. Jenie, *Spectrochim. Acta, Part A*, 2024, **307**, 123643.
39 D. Albano, K. Shum, J. Tanner and Y. Fung, *Proc. IMCS*, 2018, **2018**, 211–213.
40 N. Klippel, G. Jung and G. Kickelbick, *J. Sol-Gel Sci. Technol.*, 2023, **107**, 2–19.
41 R. Boukherroub, J. T. C. Wojtyk, D. D. M. Wayner and D. J. Lockwood, *J. Electrochem. Soc.*, 2002, **149**, H59.
42 A. B. D. Nandiyanto, R. Oktiani and R. Ragadhita, *Indones. J. Sci. Technol.*, 2019, **4**, 97–118.
43 Y. Wang, C. Jiang, G. Wen, X. Zhang, Y. Luo, A. Qin, A. Liang and Z. Jiang, *Luminescence*, 2016, **31**, 972–977.
44 O. Taratula, E. Galoppini, R. Mendelsohn, P. I. Reyes, Z. Zhang, Z. Duan, J. Zhong and Y. Lu, *IEEE Sens. J.*, 2009, **9**, 1302–1307.
45 G. T. Hermanson, *Bioconjugate Techniques*, Academic Press, 2nd edn, 2008.
46 G. Liu and Y. Lin, *Talanta*, 2007, **74**, 308–317.
47 J. Dong and H. Ueda, *Sensors*, 2021, **21**, 1223.
48 D. Song, J. Liu, W. Xu, X. Han, H. Wang, Y. Cheng, Y. Zhuo and F. Long, *Talanta*, 2021, **235**, 122800.
49 D. Darvill, A. Centeno and F. Xie, *Phys. Chem. Chem. Phys.*, 2013, **15**, 15709–15726.
50 N. Jin, S. Ling, C. Yang and S. Wang, *Toxicon*, 2014, **90**, 226–236.
51 J. Y. Eum, S. Y. Hwang, Y. Ju, J. M. Shim, Y. Piao, J. Lee, H. S. Kim and J. Kim, *Chem. Commun.*, 2014, **50**, 3546–3548.
52 H. Bai, H. Lu, X. Fu, E. Zhang, F. Lv, L. Liu and S. Wang, *Biomacromolecules*, 2018, **19**, 2117–2122.
53 R. Funari, K. Y. Chu and A. Q. Shen, *Biosens. Bioelectron.*, 2020, **169**, 112578.
54 Z. Wang, Z. Zheng, H. Hu, Q. Zhou, X. Li, W. Liu, X. Li, Z. Liu, Y. Wang and Y. Ma, *Lab Chip*, 2020, **20**, 4255–4261.
55 Q. Bayin, L. Huang, C. Ren, Y. Fu, X. Ma and J. Guo, *Talanta*, 2021, **227**, 122207.
56 K. V. Serebrennikova, N. A. Byzova, A. V. Zherdev, N. G. Khlebtsov, B. N. Khlebtsov, S. F. Biketov and B. B. Dzantiev, *Biosensors.*, 2021, **11**, 510.
57 L. Villafañe, L. G. Vaulet, F. M. Viere, L. I. Klepp, M. A. Forrellad, M. M. Bigi, M. I. Romano, G. Magistrelli, M. R. Fermepin and F. Bigi, *J. Immunol. Methods*, 2022, **500**, 13182.
58 J. Ma, M. Du, C. Wang, X. Xie, H. Wang, T. Li, S. Chen, L. Zhang, S. Mao, X. Zhou and M. Wu, *ACS Sens.*, 2021, **6**, 3367–3376.
59 W. Wu, B. T. T. Nguyen, P. Y. Liu, G. Cai, S. Feng, Y. Shi, B. Zhang, Y. Hong, R. Yu, X. Zhou and Y. Zhang, *Sens. Actuators, B*, 2022, **368**, 132198.
60 W. Wu, B. T. T. Nguyen, P. Y. Liu, G. Cai, S. Feng, Y. Shi, B. Zhang, Y. Hong, R. Yu, X. Zhou and A. Q. Liu, *Biosens. Bioelectron.*, 2022, **215**, 114594.
61 Y. Shi, Y. Wu, L. K. Chin, Z. Li, J. Liu, M. K. Chen, S. Wang, Y. Zhang, P. Y. Liu, X. Zhou and H. Cai, *Laser Photonics Rev.*, 2022, **16**, 2100197.

